Measurement Science and Technology

100 year anniversary
Measurement Science and Technology

PAPER • OPEN ACCESS

Insights into the writing process of the mask-free nanoprinting fluid force microscopy technology

To cite this article: Marcus Soter *et al* 2024 *Meas. Sci. Technol.* **35** 085605

OPEN ACCESS
IOP Publishing
Measurement Science and Technology
Meas. Sci. Technol. **35** (2024) 085605 (12pp)
https://doi.org/10.1088/1361-6501/ad44c2

Insights into the writing process of the mask-free nanoprinting fluid force microscopy technology

Marcus Soter[1], Gurunath Apte[1,2], Dikshita Madkatte[1] and Thi-Huong Nguyen[1,3,*]

[1] Institute for Bioprocessing and Analytical Measurement Techniques (iba), 37308 Heilbad Heiligenstadt, Germany
[2] Institute of Nanotechnology (INT) and Karlsruhe Nano Micro Facility (KNMFi), Karlsruhe Institute of Technology, 76131 Karlsruhe, Germany
[3] Faculty of Mathematics and Natural Sciences, Technische Universität Ilmenau, 98694 Ilmenau, Germany

E-mail: thi-huong.nguyent@iba-heiligenstadt.de

Received 13 November 2023, revised 2 April 2024
Accepted for publication 29 April 2024
Published 22 May 2024

Abstract

Platelets are activated immediately when contacting with non-physiological surfaces. Minimization of surface-induced platelet activation is important not only for platelet storage but also for other blood-contacting devices and implants. Chemical surface modification tunes the response of cells to contacting surfaces, but it requires a long process involving many regulatory challenges to transfer into a marketable product. Biophysical modification overcomes these limitations by modifying only the surface topography of already approved materials. The available large and random structures on platelet storage bags do not cause a significant impact on platelets because of their smallest size (only 1–3 μm) compared to other cells. We have recently demonstrated the feasibility of the mask-free nanoprint fluid force microscope (FluidFM) technology for writing dot-grid and hexanol structures. Here, we demonstrated that the technique allows the fabrication of nanostructures of varying features including grid, circle, triangle, and Pacman-like structures. Characteristics of nanostructures including height, width, and cross-line were analyzed and compared using atomic force microscopy imaging. Based on the results, we identified several technical issues, such as the printing direction and shape of structures that directly altered nanofeatures during printing. Importantly, both geometry and interspace governed the degree of platelet adhesion, especially, the structures with triangular shapes and small interspaces prevent platelet adhesion better than others. We confirmed that FluidFM is a powerful technique to precisely fabricate a variety of desired nanostructures for the development of platelet/blood-contacting devices if technical issues during printing are well controlled.

Keywords: insights, writing, process, mask-free, nanoprinting, fluid

* Author to whom any correspondence should be addressed.

1. Introduction

Platelet products are collected directly from human blood and stored in plastic bags before transfusion. It was reported that around 1300 l of platelet concentrate are daily transfused in Germany alone [1], and 118.54 million blood donations are annually collected globally every year [2]. In the US alone, approx. 30 000 potentially preventable deaths per year after traumatic injury due to severe bleeding [3]. Platelet transfusion demand increased because of the increase in intensive chemotherapy and hematopoietic stem cell transplantation as well as highly invasive surgical operations in several specific areas, such as cardiovascular surgery. However, above 1/2 of the US patients suffer from >1 h delay before treatment in a level 1 trauma center, and thus, lacks access to hemostatic resuscitation in the crucial minutes after injury [3]. The problem is derived from the difficulties during the management of platelet storage. Smaller hospitals generally cannot stock platelets, while in larger centers, platelet concentrates are mostly used for hematology-oncology patients only [3].

Platelets are fragments of cells that are developed from mature cell megakaryocytes in the bone marrow [4]. A single megakaryocyte can produce >1000 platelets that are stored in the spleen and blood circulation. A healthy adult contains 150 000–450 000 platelets/µl blood. Platelets are the smallest blood cells (size between 1 and 3 µm). They do not have a nucleus, and thus, are extremely sensitive. They tend to activate immediately after a short time contacting with any artificial surfaces [5, 6]. Platelet concentrates are normally pooled from 4 to 6 donor units to obtain an adult dose of at least 240×10^9 platelets [7]. Current technologies allow the storage of platelets at room temperature for only 72 h (WHO) [7]. The first problem with longer storage is the drop in pH because platelet produces a considerable amount of lactic acid and CO_2 when metabolizing glucose and consuming O_2. A low pH ultimately leads to platelet storage lesions such as platelet activation, the exhibition of apoptotic markers, and low recoveries [8]. The second problem with longer storage is the increased risk of bacterial contamination [9–12]. WHO reported that bacterial contamination affects about 1% of pooled units [7]. The short shelf life together with unpredictable demand results in platelet inventory management problems as manifested by high rates of outdating (up to 23%) [13], leading to a higher cost of platelets than other blood products such as fresh-frozen plasma or red blood cells [14]. The short storage period limits platelet transfusion in many emergency stations. According to the Blood Product Utilization Guidelines (The University of Mississippi, Medical Center), platelet transfusions may be limited only to patients with life-threatening bleeding if necessary, to preserve a limited platelet inventory [15]. During blood product shortage, the platelet transfusion thresholds will be lowered [15], that may cause higher risks for patients. If old platelets are infused in patients, a decrease in transfusion efficacy and an increase in adverse events such as transfusion-associated sepsis and immune-mediated events occur, especially, in hematology, oncology, and post-cardiac surgery patients [10]. Less than one percent of the total blood can be isolated as platelets. These problems together with the highly sensitive characteristics of platelets lead to extreme difficulties during storage management. Stored platelets after collection may become deactivated or dysfunctional towards the end of the storage time [16]. As a consequence, the total cost of platelet transfusions in a US hospital inpatient setting was raised to 1360$ per platelet unit [16]. Thus, an extension of the shelf life for platelet storage has both positive financial and inventory management outcomes.

Regarding platelet storage improvement, an important effort to introduce microtextures either on one or both sides of the bags has been developed to prevent the inside faces from sticking during heat sterilization or processing [17]. However, these microstructures exhibit several limitations such as the enhancement of platelet adhesion and bacterial growth [18, 19]. Adherent platelets immediately activate and transform into filopodia and lamellipodia [20], causing several bioactive chemicals to be released, which may lead to platelet aggregation or breakdown in bags. This further enhances the drop of pH in the platelet bag [20]. A similar or even more complicated thrombogenic mechanism can occur on many medical devices such as transfusion apparatus and implants [21]. It has been reported that platelet adhesion/activation on an implant obstructs the functionality of the materials and causes blood vessel narrowing [22, 23]. Consequently, patients who receive implants are often given high doses of anticoagulants [24]. Venous catheters, vascular grafts, stents, and heart valves have been previously associated with thrombotic complications, resulting in failures, body rejections, or even stroke and heart attacks [25]. Thus, the material-blood interaction is critical in determining the body's acceptance of the implants [26]. As the contact adherence of platelets on biomaterials is the first step in the formation of a thrombus [27], minimizations of surface-induced platelet activation play a crucial role in the development of ideal blood storage bags and overcoming current limitations in platelet-contacting devices. For decades, the improvement of blood-contacting materials has still been suffering from major challenges [28].

While microstructures have only a minor effect on platelets, nanostructures that are placed directly underneath the platelets can govern cellular response. However, currently, available technologies for the fabrication of nanostructured surfaces using commercially available synthetic as well as bio-based mono- and polymers are limited. Even though two-photon polymerization (2PP) allows to print structures down to 100 nm [29, 30], the technique is time-consuming, complex, inefficient for fabrication of a large sample size, and only works with photo-polymerizable materials. The mask-free FluidFM-based atomic force microscopy (AFM) technology is a versatile method for generating functional and topographical features ranging from synthetic [30, 31] to biological materials [32]. The use of the FluidFM enables the cost- and time-efficient production of almost limitless prototype structures. Previously, we have demonstrated the feasibility of the FluidFM in printing dot-grid and hexagonal nanostructures using a commercial hybrid acrylate-based UV curable Loctite AA3491 (Henkel) [31]. These structures caused a reduction of

surface stiffness and inhibited platelet adhesion and activation. As the best structures that exhibit the highest ability for anti-platelet adhesion have not yet been identified, we aim in this study to fabricate several structures of different features. We hypothesized that the platelet-like structures may be the most suitable for anti-platelet adhesion expectations. Therefore, we aim here to fabricate platelet-like structures including circle, triangle, and Pacman-like structures, and compare them with non-platelet-like grid features. We demonstrated that FluidFM allows the fabrication of nanostructured surfaces of varying features with superimposed printing for increasing height, however, printing direction influenced the resulting structures. By characterizing the height, width, and transverse line, of the printed nanostructures, and comparing them, we identify that printing direction, shapes of structures, and tip-effect directly altered nanofeatures during printing. Our results indicate that FluidFM is a powerful fabrication technique to produce a variety of desired nanostructures for the development of platelet/blood-contacting devices if the printing parameters and technical issues are well controlled.

2. Methods

2.1. Ethics

Human blood obtained from healthy volunteers including the informed consent procedure was approved by the ethics board at the Thüringen, Germany. All volunteers gave informed consent.

2.2. FluidFM based printing

The structures were printed using a Nanowizard 4 setup (JPK, Berlin, Germany) with a FluidFM add-on (Cytosurge, Opfikon, Switzerland), placed under an acoustic hood, and mounted on an active vibration isolation system (Micro 40, Halcyconics, Germany) to mitigate the effect of external vibrations. The cantilever was observed and moved to the desired spots using an inverted microscope (Axio Observer Zeiss, Jena, Germany). Before printing, the structures were first designed using Inkscape (version 0.17), an open-source vector-based graphics application that enables users to create and modify the desired pattern to an exportable scaled vector graphic file (SVG). This pre-designed structure was imported into the AFM control program JPK Nanowizard4. As print material, the commercially available Loctite AA3491 (Henkel, Düsseldorf, Germany), made up of a combination of different methacrylate esters that polymerize when exposed to UV light was filled in the reservoir of microchannel cantilever, was used. The Loctite AA3491 is composed of monomers from isobornyl acrylate, 2-hydroxyethyl methacrylate, acrylic acid, and hydroxypropyl acrylate [33]. Before each printing cycle, a nanopipette with an aperture of 300 nm and a nominal spring constant of 2 N m^{-1} (Cytosurge, Opfikon, Switzerland) was calibrated using the contact-free thermal noise method before being approached to the surface. In manipulation mode, the structures were printed on a glass coverslip (Plano GmbH, Wetzlar, Germany) of 24 mm which was pre-cleaned with 80% Ethanol under 30 min sonication. The printing was done in an area of 100 × 100 μm by upholding a steady positive pressure of 20 mbar, set point of 20 nN, and writing speed of 12 μm s^{-1} at ambient controlled conditions, i.e. 22 °C, humidity 35%, and atmospheric flow of 25 m^3 h m^{-2}. For polymerization, the samples were cured after printing using a UV lamp at 365 nm for 5 min.

2.3. Characterization of printed structures using AFM

In order to determine the dimension of the printed nanostructures such as height, width, and interspaces as well as the changes in structures during printing, we imaged the samples using AFM. As AFM provides an atomic resolution, detailed changes caused by printing directions or raised by specifically designed structures could be visualized. The AFM topological images were obtained by scanning surfaces in contact mode. All the samples were imaged using a cantilever from Bruker (MLCT-Probe A) with a nominal spring constant value of 0.07 N m^{-1} at a line rate of 0.3 Hz and a resolution of 512 × 512 pixels and a scan size of 100 × 100 μm. Using JPK software (JPK Nanowizard4) for analysis, the line profiles of the features were accomplished by selecting the image cross-section option to determine the size of each printed feature. To calculate the mean value and the standard deviation, at least 25 individual measurements on each of the 3 repetitions per structure geometry were examined. The boxplot diagrams were created using Origin, Version 2023b. (OriginLab Corporation, Northampton, MA, USA). The whiskers represent the 1.5 IQR and the box represents the 50% value.

2.4. Platelets extraction from blood

Blood was drawn into a 10 ml blood collecting tube containing 1.5 ml acid-citrate dextrose ACD-A (BD-Vacutainer, Berlin, Germany) from healthy human donors who had not consumed any drugs in the previous two weeks. The blood tube was sealed with parafilm, inclined at an angle of 45°, and rested at room temperature for 15 min before centrifugation. Firstly, blood was centrifuged at 120 g for 20 min at room temperature to separate platelet-rich plasma (PRP) from the blood. Further, platelet isolation from PRP was accomplished by centrifuging at 650 g for 7 min in a buffer containing 11% ACD-A (Fresenius Kabi, Germany) and 2.5 U ml^{-1} Apyrase (grade IV SIGMA, Munich, Germany). The platelet pellet was resuspended in 1 ml of suspension buffer at pH 6.3, consisting of 137 mM NaCl, 2.7 mM KCl, 11.9 mM $NaHCO_3$, 0.4 mM Na_2HPO_4, and 2.5 U ml^{-1} Hirudin. Following that, an additional 4 ml of suspension buffer was added, and the platelets were incubated at 37 °C for 15 min. The suspension was then centrifuged again for 7 min at 650 g. Following a second resuspension of platelet pellets in 2 ml of suspension buffer, platelet counting was carried out using a blood counter (pocH-100i, SYMEX, Germany). In the suspension buffer, the platelet concentration was further adjusted to 30 000 μl^{-1} for sample stabilization and rested at 37 °C for 45 min before use.

2.5. Platelet adhesion on bag surfaces

The platelet adhesion on a plastic bag was performed to get an insight into platelet activation on a commercially available storage bag (Terumopenpol, Thiruvananthapuram, India). A Storage bag pieces of 1 × 1 cm were cut from the bag and cleaned under UV ozone for 30 min. After that, platelets of 30 000 μl^{-1} were added to bag pieces and incubated for 1 h After rinsing with phosphate buffer saline (PBS) to eliminate any remaining unbound platelets, 4% Paraformaldehyde (PFA) was added to fix the platelets. After fixation, the platelets were stained for 1 h with an anti-CD42a FITC antibody (Dianova GmbH, Hamburg, Germany) at a final concentration of 1 $\mu l\ ml^{-1}$ of platelet solution to quantify the adherent platelets on the surface. The sample was then washed twice with PBS to remove the unbound dye before examining by the confocal laser scanning microscopy Zeiss LSM710 (Carl Zeiss, Gottingen, Germany) at room temperature in the dark. The fluorescent signal was acquired at an excitation/emission wavelength $\lambda = 495/518$ nm using a 63x objective. Also, a T80/R20 beam splitter was used for taking images to perform confocal reflection microscopy on the patterns. The size and quantity of the platelets were determined using ImageJ (ImageJ 1.54d, Wayne Rasband and contributors National Institute of Health, USA). The appropriate threshold was first selected and the size and number of platelets were determined using the particle analyzer available in the program. To quantify the amount of adherent platelets and their average spreading, the mean and standard deviation of three structures per geometry incubated with platelets from one donor, were calculated.

3. Results and discussion

3.1. Dissimilar response of platelets on micro- and nanostructures

To identify the dissimilar effect of micro and nanostructures on the response of platelets, we compared the response of platelets on these structures. A commercially available bag that contains microstructures was tested. Platelets were incubated on this bag and stained P-selectin using CD42a FITC antibody for imaging with a confocal microscope. A high density of platelets adhered to the bag, both on microstructures and outside the structured surfaces (figures 1(A)–(C)). A similar observation was also reported in the literature [18, 19]. This clearly shows no effect of large structures on the inhibition of surface-induced platelet adhesion. As any adhered platelets will be activated quickly [20], they release from their intracellular granules namely dense granules, multiple bioactive molecules such as adenosine diphosphate (ADP), adenosine triphosphate (ATP), guanosine 5′-[β-thio]diphosphate (GDP), 5-hydroxytryptamine (5-HT) and PF4. These bioactive molecules further trigger platelet adhesion by signaling positive feedback and cause activation of integrin αIIbβ3 and fibrin which lead to the formation of a thrombus or a platelet plug. This can cause aggregation/degradation and alter the storage buffer over time [8, 32]. Bacterial film formation on this type of bag has been also reported [18, 19]. Thus, the commercially available structured surface does not inhibit platelet adhesion/activation or improve platelet storage.

We have previously proven that the commercial hybrid acrylate-based UV curable Loctite AA3491 (Henkel) allowed the printing of several types of nanostructures such as hive (=hexagonal) features (figure 1(D)) [31, 33]. These nanostructures strongly reduce platelet adhesion as shown by a low density of platelets (figure 1(E)) compared with a high density of cells on the nonstructured polymer film (figure 1(F)). Our findings demonstrated the important role of nanotextures in the inhibition of platelet-surface adhesion and activation. However, we have so far only been successful in printing dot-grid and hive structures. In the next section, we report challenges in the fabrication of nanostructures with multiple features.

3.2. Design for mask-free nanoprinting with fluid force microscope (FluiFM)

To print other types of nanostructures, we used here FluidFM and also a commercial hybrid acrylate-based UV curable Loctite AA3491 (Henkel) ink. The ink was injected in a microchannel probe connected with a tip aperture of ∼300 nm. By applying a pressure of 20 mbar, the ink was pushed through the aperture to generate nanostructures (figure 2(A)). The structures were cured under a UV source at 365 nm wavelength. Figure 2(B)). As previously observed hexagonal (=hive) structures show effective platelet inhibition compared to dot-grid structures [31], here we printed other structures with platelet-like shapes including grid, circle, triangle, and Pacman-like features. We hypothesize that the continuous and symmetrical features are favorable surfaces for platelets because they generate a homogeneous and gentle matrix underneath them and thus, reduce platelet adhesion and activation. Importantly, by printing these designed structures, we aim to understand the feasibility of FluidFM in printing various complexities of structures. Within these designed structures, the FluidFM cantilever must move in a linear and nonlinear direction and the contact angle of the tip is changed during printing. This effect has not been thoroughly understood in the literature yet.

3.3. Fabrication of structured surfaces of different features

To fabricate the structures, ink was loaded into the microchannel probe connected to a cantilever with a tip aperture of ∼300 nm. The designed structures were loaded into the JPK software for printing under manipulation mode. By applying pressure, the ink from the microchannel probe was pushed through the cantilever aperture for printing the patterns. We have successfully printed four types of structures including grid, circle, triangle, and Pacman-like as viewed by light microscopy images (figure 3(A)). AFM images allow determination of the height and width of the structures (figure 3(A)) *via* analysis of line profiles. We compared those parameters among the printed structures (figure 3(B), white lines). In figure 3(C), the corresponding height profiles are shown.

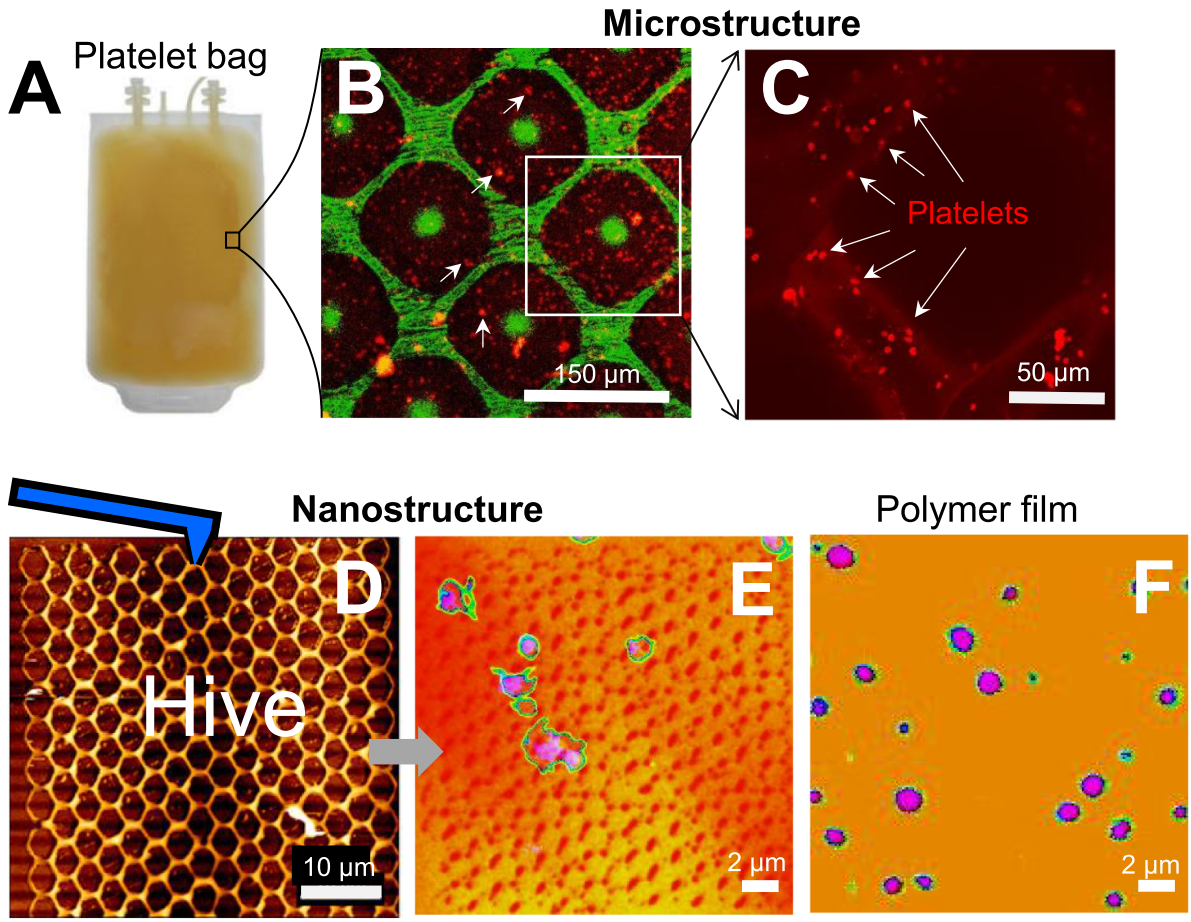

Figure 1. Distinct adhesion phenomenon of platelets on micro- and nanostructures. (A) Platelet concentrates are collected from healthy blood donors and stored in commercially available structured plastic bags before transfusing to life-threatening bleeding patients. (B) Platelets in red (arrows, *stained with anti-CD42a FITC*) adhered and aggregated on nonstructured surfaces while green indicates microstructures on the bag surface. (C) The enlargement shows multiple platelets also adhered to the structured surfaces (arrows). (D) Atomic force microscopy of nanostructures with hive (=hexagonal) features printed with FluidFM. (E) Confocal reflection microscopy of hive features shows a strong reduction of platelet adhesion (marked by the green boundary) as compared with (F) nonstructured polymer film of the same material. In E, Platelet actin fibers and CD42a expression were correspondingly stained by DY590 phalloidin (red) and anti-CD42a FITC-conjugated antibody (blue), merged with images of the structure which were taken by setting the filter T80/R20 in CLSM, and post processed while platelet bodies were emphasized by pink color for visualization. Round shapes indicate nonactivated platelets whereas activated platelets expose random shapes adapted from [31]. Reprinted with permission from Apte *et al* [31], copyright 2022 American Chemical Society.

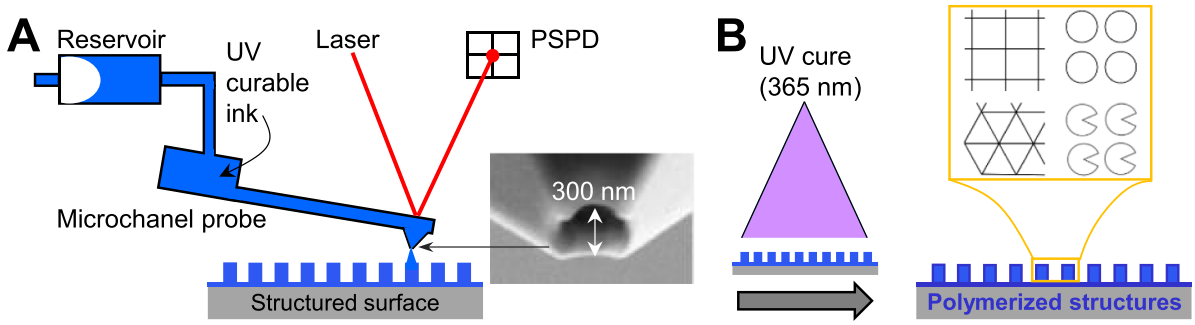

Figure 2. The scheme shows the principle for the fabrication of nanostructured surfaces using FluidFM. (A) FluidFM prints structures using UV-curable ink injected in a microchannel probe (blue) with a tip aperture of ∼300 nm. By applying a force to the cantilever together with pressure through the reservoir, a pattern of designed structures will be printed in a force-manipulation mode. (B) The structured surface is formed after UV curing at a wavelength of 365 nm. Platelet-like features including grid, circle, triangle, and Pacman-like structures are printed.

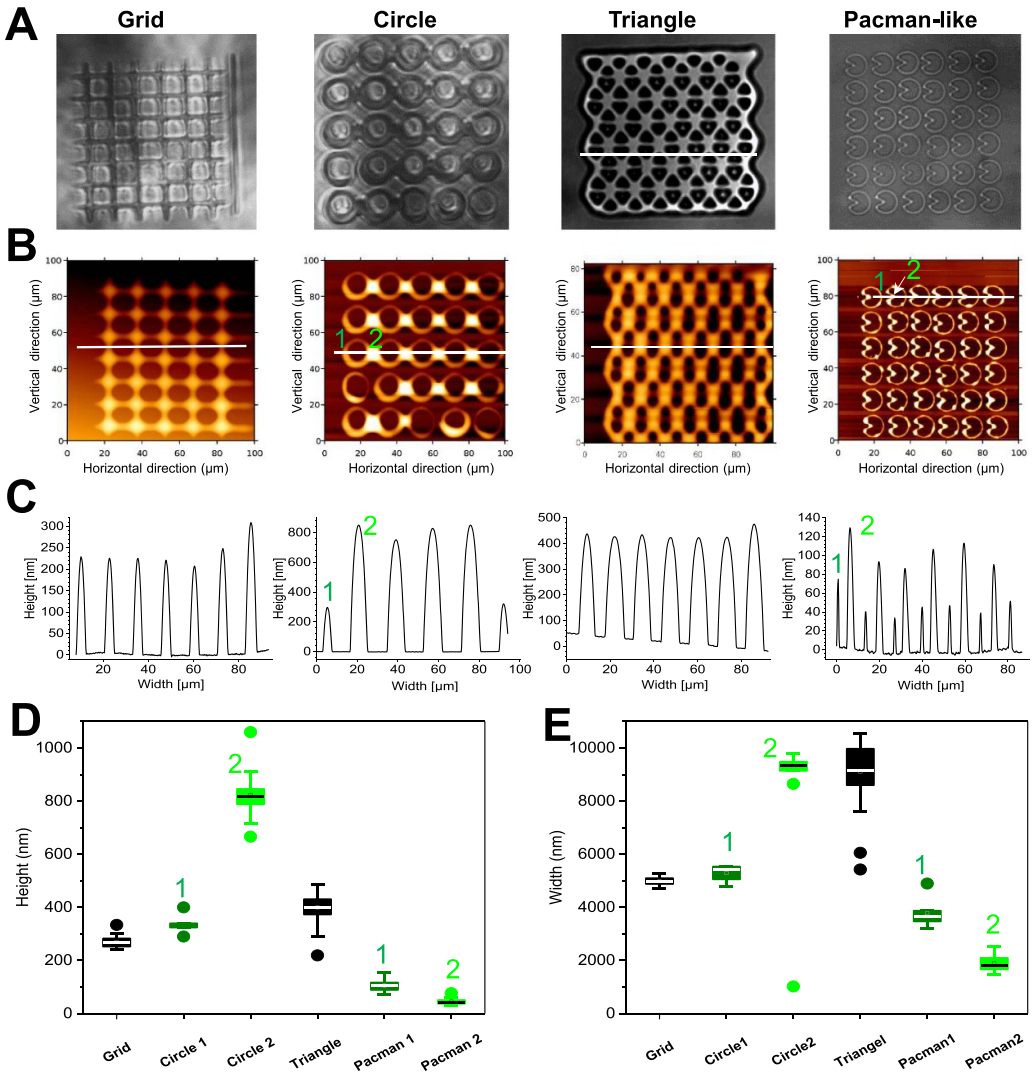

Figure 3. Fabrication of nanostructures of different features by FluidFM. (A) Light microscopy images show four platelet-like features including grid, circle, triangle, and Pacman-like structure. (B) AFM images and (C) Height changes at the corresponding line profiles were taken horizontally on the structures. (D) Height and (E) width values collected from different line profiles differed among printed structures. Circle and Pacman-like showed two distinct heights point-1 and 2 (green, (B)–(D)).

Data collected from different line profiles are presented as box plots for height (figure 3(D)) and width (figure 3(E)). For all measurements, a relatively low variation of measured height/width was observed, indicating a good reproducibility of the FluidFM in fabricating micro-/nanostructures. However, both height (figure 3(D)) and width (figure 3(E)) changed depending on the feature of the designed structures. Additionally, the height, as well as the width in individual structures, was not uniform. For the grid, the structures are rather uniform (226.0 $\pm$ 21.2 nm) (figure 3(D)). The circles show two distinct heights (point-1 and point-2, figures 3(B)–(D)) in which point-2 displays the merging of two close circles. Triangle lines are higher than the grid, circle-1, and Pacman height. The Pacman-like structures also show two different heights (point-1 and point-2, figures 3(B), (C) and (E)). Among these structures, the heights vary up to 400 nm, except for the merging of the circles at point-2. The widths at these analysis points also varied depending on the features of structures (figure 3(E)). Our results indicate that the printing direction caused by the features of the desired structures plays an important role in the resulting dimension of the structures.

3.4. Insights into nanoprinting process

To gain insights into the process while nanoprinting, we enlarged the structures and compared the width, height, and also cross-section for each type of feature by analyzing AFM line profiles (figure 4). Figure 4(A) shows 3D (top panels) and 2D (low panels) images with changes of printing lines depending on printing direction (white arrows) and features of structures. To understand the effect of printing direction, we compared the structural height and width in the vertical or horizontal direction (figures 4(A)–(D), blue and green lines, respectively). To gain insight into the layer-by-layer printing procedure, we analyzed the cross-section at the knots

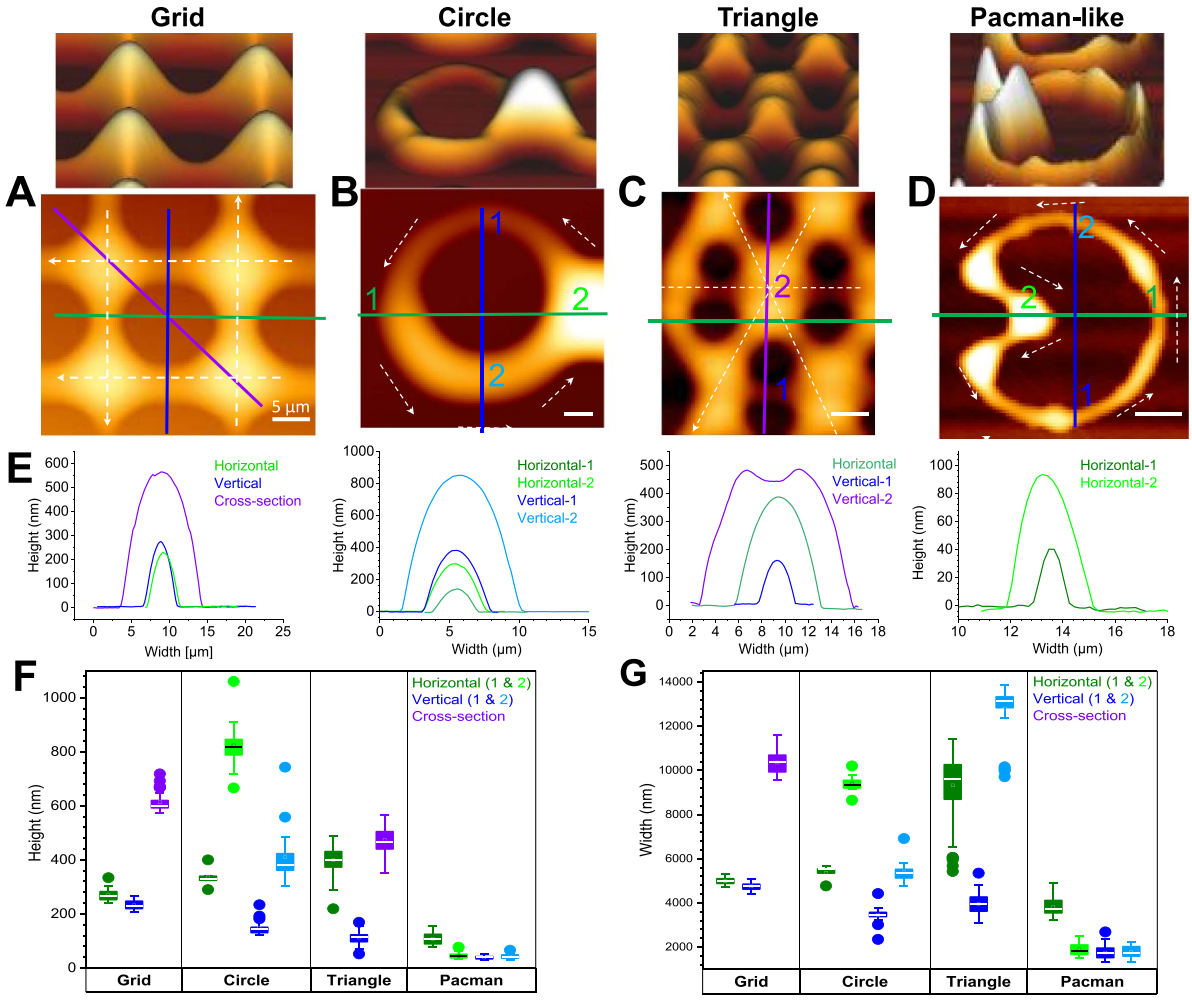

Figure 4. Effect of printing direction and features of structures on printing results. (A) 3D (top panels) and 2D (lower panels) images taken by AFM show the changes in printing size depending on the printing direction (white arrows) and the features of structures. Analysis of line profiles of the structures measured horizontally (green) or vertically (blue), and at the knots where two ((A), violet) or three ((C), violet) printing lines are superimposed. The unequal ink distribution while printing (B) Circles and (D) Pacman-like structures were compared by analysis of image line profiles. (E) Comparison of line profiles at different positions for each structure showed dissimilar heights and widths. (F) Height and (G) Width from all printed structures at different analysis positions showed significant changes in structures.

(figures 4(A) and (C), violet lines) where up to three printing lines were superimposed.

For grid structure, printing in the vertical direction resulted in a lower height (220 ± 16 nm) than in the horizontal direction (266 ± 21 nm). A similar effect for the width, 4759 ± 162 nm in the vertical direction and 4985 ± 131 nm in the horizontal direction was observed (table 1). The results indicate that the writing direction caused changes in the dimensions of the designed structures. This effect could also be seen in the triangular shape. The height of single lines in the vertical direction of the triangles is approximately the same as that of the grid. However, much larger width (9616 ± 1362 nm) and higher height (401 ± 47 nm) were seen in the horizontal direction which can be explained by the merging of two printing lines. The influence of the writing direction becomes more interesting when analyzing the circular structures. Within a circle, both height and width at point-1 differ from those at point-2. At point-2, a high amount of ink was transferred to the substrate, resulting in merged structures of two close circles. Therefore, the height and width at point-2 in the horizontal direction display the value for the merged structures. The shape of the cantilever also likely played a role. Probably, the non-flat, asymmetric end of the tip aperture led to unequal output of ink when the cantilever printed the different angles. This resulted in a highly different amount of ink (either less or more) distributed to the substrate, leading to a large variation within a circle (818 nm *vs* 329 nm in height and 5528 nm *vs* 3943 nm in width corresponding to measurements at point-2 and point-1). The Pacman-like structures are a combination of line and circular shapes. In comparison to circles or lines only, the height and width of Pacman-like structures are reduced. At the circular part, the height is approx. 40 ± 10 nm which is only about 10% of the height of the circular-shaped structures without lines. Besides, the line part has a height of 107 ± 17 nm and width of 3737 ± 379 nm which is lower than those for lines only in grid or triangle structures.

Table 1. Width and height depend on printing structures and measuring points.

Structure		Height (nm)	Width (nm)
Grid	Horizontal	226.0 ± 21.2	4985.0 ± 131.5
	Vertical	228.5 ± 15.7	4759.0 ± 162.4
	Cross-Section	601.0 ± 27.9	$10\,380.0 \pm 529.7$
Circle	Horizontal-1	329.0 ± 35.7	5528.0 ± 317.2
	Horizontal-2	818.0 ± 80.9	3943.5 ± 327.4
	Vertical-1	143.5 ± 24.7	3457.0 ± 332.4
	Vertical-2	380.5 ± 86.7	5339.0 ± 407.2
Triangle	Horizontal	401.0 ± 46.5	9616.0 ± 1362.2
	Vertical-1	113.5 ± 24.0	3942.0 ± 489.0
	Vertical-2	466.5 ± 41.7	$13\,145.0 \pm 1076.5$
Pacman	Horizontal-1	107.0 ± 17.2	3737.0 ± 379.3
	Horizontal-2	43.0 ± 9.8	1803.0 ± 271.8
	Vertical-1	39.0 ± 5.1	1725.0 ± 282.2
	Vertical-2	41.0 ± 8.0	1728.0 ± 240.9

Our results indicate the influence of the tip geometry and printing direction while writing structures of different geometries. As shown in figure 2 (inset), the geometry of the probe is not equal in all directions. The cantilever has a rather straight opening on one side while it has a semicircular opening on the other side. Due to the shape, the amount and output of ink in the different directions are influenced. This means that the amount of imprint resin applied depends on the writing direction while the orientation of the cantilever remains the same. The tip effect had little impact on the grid structure, but it had a significant impact on the circular-shaped structures, resulting in printed features that were dissimilar from the desired structures. In contrast to lines, the circular structures, displayed all directions at once while all the angles of the probes were used in order to write a circle. It can be seen that the amount of ink distributed to the substrate was guided by the movement direction of the FluidFM probe. The semi-circular opening allows a higher ink application and higher structure heights on point Vertical-2 while at Vertical-1, the flat side of the cantilever results in a lower application of ink. A similar effect is observed with the triangular structure. Whereas with the horizontal line, imprint resins are applied to the glass substrate via the straight side as well as the semicircular side with the vertical lines. For the circle structures, this effect is so great that the structures even converge in the horizontal direction. The geometric differences could be partially compensated for by adjusting the imprint pressure and the imprint speed in the respective directions. In addition to the geometry of the cantilever, these two parameters are largely dependent on the amount of ink applied. By reducing the imprint pressure or increasing the imprint speed in areas where the semicircular opening of the cantilever significantly influences the ink application, a lower height and thus a more uniform height and width of the structures could be achieved. In addition, the alignment of the cantilever could be adjusted by rotating the AFM head so that the application direction remains the same as the direction of the cantilever. However, this is not possible with our current setup.

Table 2. Effect of setting parameters during FluiFM printing [31].

Printing parameters	Effect on the width of structures	Range
Contact time	Strong	$\leqslant$20 s
Writing velocity	Strong	$\leqslant$2.2 μm s^{-1}
Setpoint	Weak	$\leqslant$20 nN
Pressure	Weak	$\leqslant$70 mbar

Our observation is in line with a previous study showing the influence of the printing direction on the linewidth in which a direction-dependent difference in the height increased up to 10-fold [34]. However, this study only reported the impact on printing lines. The height of the printed lines was only between 10–20 nm. In our work, a significantly higher height and width can be shown even though the same Loctite ink was used. This difference can be due to the printing parameters used such as printing speed and tip contact time. We have previously found that printing speed and contact time have a major effect on the size of the structures whereas other parameters such as setpoint and applied pressure do not cause a significant change (table 2) [31].

Besides this, it must be taken into consideration that while printing the lines in manipulation mode, the FluidFM probe moved in one x (or y)-direction only while the y (or x)-direction was fixed. When printing circles, the tip moved with small steps in both x and y-directions to fulfill a circular shape. These different processes between printing lines and circles can be recognized better when combining them in the Pacman-like structure that is a combination of both lines and circles. The amount of ink applied in the circular part was much less than for circles only. Here, it seems that the tip contacted the substrate during printing at both linear and circular parts.

It should also be noted that with Pacman-like structures, corners are printed. The cantilever stays at the corner point for a short moment before moving in the next direction. This results in an increased application of ink at the corners. Due to the increased application of ink in the corners, less ink is applied in the round areas of the Pacman-like structures because the cantilever pushes less ink in front of it.

Besides narrow width, the higher height of the structures can prevent the platelets from contacting with the substrate, and thus, reduce platelet activation. In principle, the height can be increased by layer-by-layer deposition. In our designed grid and triangle structure, the knots (=crossed areas) are composed of superimposed writing lines that can be considered as a double layer. In comparison to printing one line, the crossed area where two times ink was applied, shows a higher height (601 ± 28 nm) compared to the combined/sum height of both vertical (228 ± 16 nm) and horizontal (266 ± 21 nm) lines when printed separately.

While with a single-layer imprint, the ink is applied to the glass substrate, with a two-layer imprint the ink is applied to ink. Of course, the adhesion between inks on the substrate and inks also differs. The results allowed to conclude that the adhesion of the ink to ink is higher, and therefore, there is an increased application of ink. In addition to the differences in

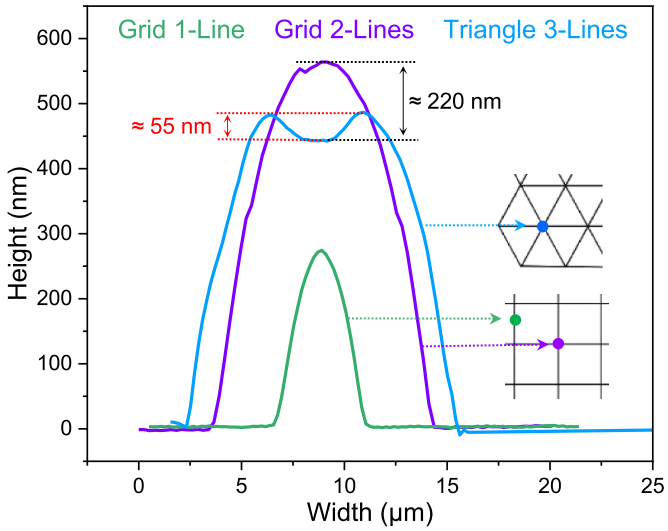

Figure 5. Differentiation between the height occurred by printing one (grid, green), two (grid, purple) and three (triangle, blue) layers.

adhesion, there is also a mechanical influence. The already-applied ink line serves as an obstacle for the AFM cantilever. This means that when the cantilever reaches such an obstacle, the well-known edge-pinning effect can occur, which can result in an increased amount of ink application. This effect can be reinforced by the sticky ink, which means the cantilever sticks even more strongly to the existing obstacles.

For triangles, in the cross knot area, it was three times printed but the height of the 3-fold single line print was not seen. Here, the height was even reduced (about 220 nm, figure 5) compared to the double height of two single lines. Interestingly, the line profile at the cross area in the triangles shows a valley (approx. 55 nm) on the top of the structures (figure 5). The first two applications of ink likely led to a rise in the height but the third one was not successful. Instead of adding ink, the tip took away some nanodrop of ink, leaving a groove at the top of the structures, leading to a reduction in height. It seems that the previously printed ink layer was at the starting phase of drying. Under an applied force, the tip indented the already partially dried structures, leaving a depth valley. Approaching the tip to the intermediate soft-hard interface, the open apertures of the cantilever seemed to be 'closed' by the partially dried flexible material. This resulted in no ink being transferred to the post-printed structures. In order to create the same conditions, each layer would first have to be cured individually. This could also prevent the cantilever from penetrating and forming a valley. The disadvantage of this, however, is that the AFM head over the sample has to be removed, and it is, therefore, possible that the old position is not exact when repositioning, and therefore superimposed printing is not possible.

To prevent this, the optimal ink viscosity and the time lag between the printing layers should be precisely adjusted. Furthermore, the volume of the ink required to deposit on each additional layer may differ and needs more optimization. Probably, when the structure becomes thicker by multiple additional layers, a higher ink volume is required to cover the whole surface of the post-printed structures.

In comparison to Ventrici De Souza *et al* who showed an increase in height by printing two layers [34], we were also able to demonstrate an add-up of 2 layers while printing. The authors reported an increased height of the second layer of only 20% whereas we were able to show an increased height of the second layer up to 50% (figure 5). We postulate that due to our low printing speed (12 µm s^{-1}) compared with the faster printing (50–200 µm s^{-1}) in the study of Souza *et al*, the contact time between ink and substrate as well as between ink and ink was increased, leading to an enhanced adhesion among the old, newly added ink and the substrate.

Our study however has several limitations. Even though the environmental conditions are well controlled, minor changes in temperature, humidity, and atmospheric flow may contribute to the resulting printed dimensions. These small changes may result in large variations while printing micro/nanostructures by AFM using Loctite ink. These limitations are not possible for investigation at our laboratory. Optimization may help to avoid artifacts during printing, e.g. varying temperatures can probably tune the structural dimensions.

3.5. *Platelet adhesion on printed structures*

To investigate the influence of the structures on the degree of platelet adhesion and activation, a solution of platelets (30 000 Plt/µl) was added to the structures including grid (figure 6(A)), circle (figure 6(B)), triangle (figure 6(C)), Pacman-like (figure 6(D)), and glass as control (figure 6(E)) and allowed to incubate for 15 min. After fixing and staining the platelets, the number of adhered platelets and their average sizes were examined to compare the degree of cell adhesion/activation induced by the same area of structures (figure 6(F)).

In addition to the geometrical effect, we also observed an influence of interspacing. The round structures circle and Pacman-like show reduced adhesion compared to the grid structures with the same interspacing. Despite the angular geometry of the triangles, these structures still exhibited reduced platelet adhesion. This could be due to the reduced interspacing (approx. 3 µm in contrast to approx. 8 µm for grid circle and Pacman-like), leading to reduced platelet-glass contact possibilities. Even in comparison to the significantly larger structures on commercial blood bags (figures 1(A)–(C)), a reduction in the number of platelets can be observed. To further reduce platelet adhesion and spreading further investigation and optimization should be carried out with the angled (low spreading) structures with reduced interspacing. An investigation of different interspaces with the same structure could provide further insights into the behavior of the platelets concerning the angularity of the possible structures.

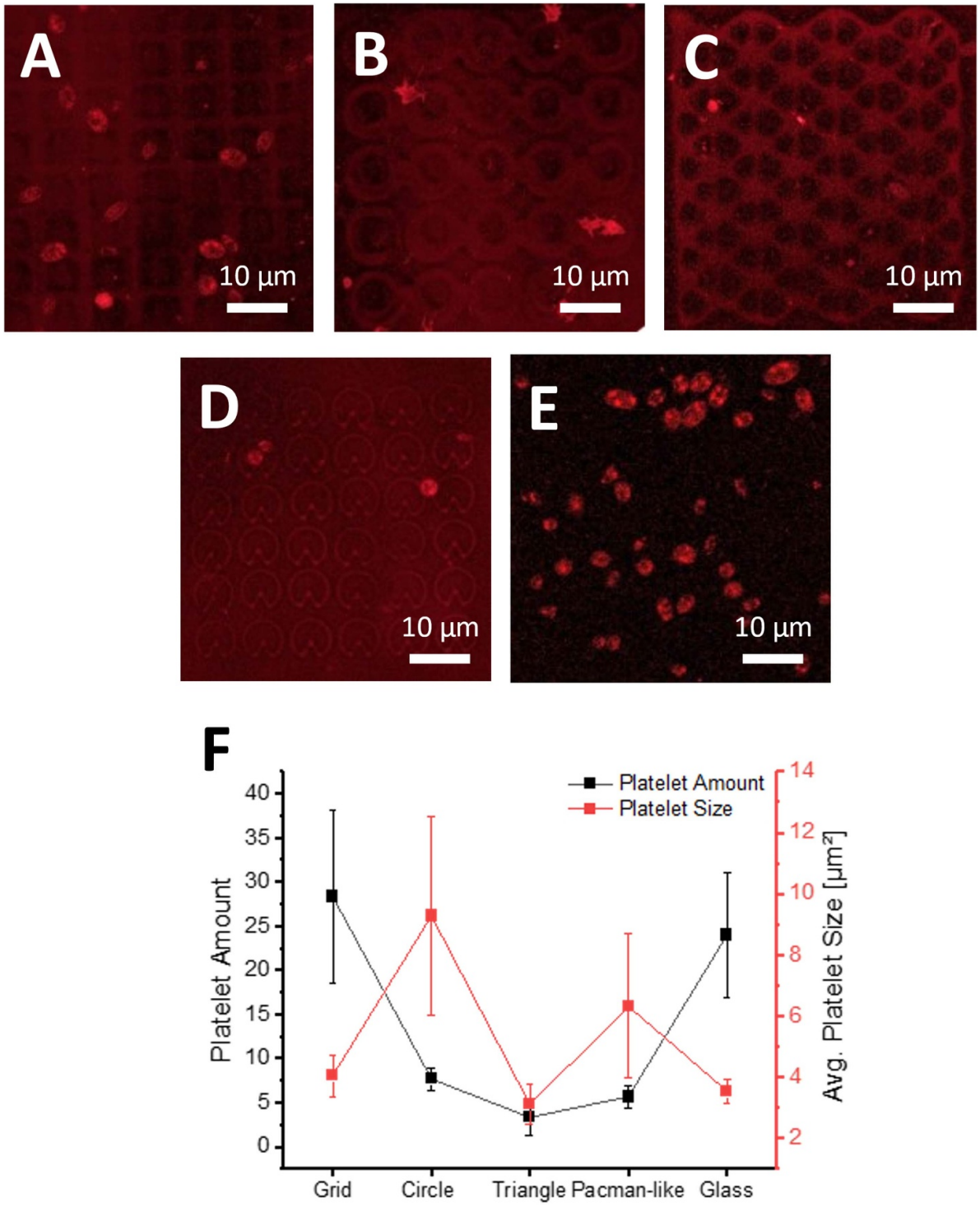

Figure 6. Platelet adhesion and spread on printed structures. (A)–(E) Confocal scanning microscope images of the adherent platelets (red, stained with anti-CD42a FITC) on the grid (A), circle (B), triangle (C), Pacman-like (D) structures, and glass as a control (E). (F) Quantification of the number and average size of adherent platelets on the different structures. The adhesion on the triangular structures is lowest. The round, circle, and Pacman-like structures, also show a significantly reduced adhesion to platelets compared to the grid structures and the glass substrate.

4. Conclusion

We demonstrated that FluidFM allows to fabricate nanostructures of different features. Characteristics of structured surfaces including height, width, and cross/knots varied depending on the printing direction and the features of the designed structures. FluidFM printed precisely simple and straight structures but unequal height and width of the structures were observed when printing circles, triangles, and Pacman-like shapes. We explained the causes

of nonhomogeneous structures and suggested a solution to overcome the identified technical issues caused by printing direction and complex shapes. In comparison with previous studies, we could produce structures of higher height utilizing a layer-by-layer platform. The adhesion of platelets is influenced by the geometry and the interspacing. We confirmed that FluidFM is a powerful technique to precisely fabricate a variety of desired nanostructures for the development of platelet/blood-contacting devices. To fabricate optimized micro/nanostructures, numerous technical issues during printing should be controlled. This provides new approaches for future studies to understand the interactions of platelets with structure surfaces and to improve the storage time and availability of platelet transfusions.

Data availability statement

All data that support the findings of this study are included within the article.

Acknowledgments

We acknowledge the support of the Freistaat Thüringen (Thüringer Ministerium für Wirtschaft, Wissenschaft and Digitale Gesellschaft, TMWWDG, Germany) and the support of the German Research Foundation (DFG) within the Projects (Nr. 469240103).

Author contributions

M S printed the structures, analyzed the data, discussed the results, and wrote the manuscript. A G performed platelet adhesion on the plastic bag. D M designed Pacman-like structures. T H N developed the study concept, discussed the results, performed the supervision, administered the project, acquired the funding, and wrote the manuscript. All authors have read and agreed to the final version of the manuscript.

Conflict of interest

The authors declare no conflict of interest.

ORCID iDs

Marcus Soter https://orcid.org/0009-0004-5653-0489
Gurunath Apte https://orcid.org/0000-0002-4391-2152
Thi-Huong Nguyen https://orcid.org/0000-0002-9237-3482

References

[1] Vit G, Klüter H and Wuchter P 2020 Platelet storage and functional integrity *J. Lab. Med.* **44** 285–93
[2] WHO Blood safety and availability (Accessed 26 May 2022)
[3] Cap A P and Spinella P C 2017 Just chill-it's worth it! *Transfusion* **57** 2817–20
[4] Mcdonald T P 1989 The regulation of megakaryocyte and platelet production *Int. J. Cell Cloning* **7** 139–55
[5] Bui V C, Medvedev N, Apte G, Chen L Y, Denker C, Greinacher A and Nguyen T H 2020 Response of human blood platelets on nanoscale groove patterns: implications for platelet storage *ACS Appl. Nano Mater.* **3** 6996–7004
[6] Nguyen T H, Palankar R, Bui V C, Medvedev N, Greinacher A and Delcea M 2016 Rupture forces among human blood platelets at different degrees of activation *Sci. Rep.* **6** 25402
[7] Czich S, Wloka T, Rothe H, Rost J, Penzold F, Kleinsteuber M, Gottschaldt M, Schubert U S and Liefeith K 2020 Two-photon polymerized poly(2-ethyl-2-oxazoline) hydrogel 3D microstructures with tunable mechanical properties for tissue engineering *Molecules* **25** 21
[8] Dekkers D W C, De Cuyper I M, Van Der Meer P F, Verhoeven A J and De Korte D 2007 Influence of pH on stored human platelets *Transfusion* **47** 1889–95
[9] Sahler J, Grimshaw K, Spinelli S L, Refaai M A, Phipps R P and Blumberg N 2011 Platelet storage and transfusions: new concerns associated with an old therapy *Drug Discovery Today: Dis. Mech.* **8** e9–e14
[10] Aubron C, Flint A W J, Ozier Y and McQuilten Z 2018 Platelet storage duration and its clinical and transfusion outcomes: a systematic review *Crit. Care* **22** 185
[11] Levy J H, Neal M D and Herman J H 2018 Bacterial contamination of platelets for transfusion: strategies for prevention *Crit. Care* **22** 1–8
[12] Arman M, Krauel K, Tilley D O, Weber C, Cox D, Greinacher A, Kerrigan S W and Watson S P 2014 Amplification of bacteria-induced platelet activation is triggered by FcgammaRIIA, integrin alphaIIbbeta3, and platelet factor 4 *Blood* **123** 3166–74
[13] Flint A W, McQuilten Z K, Irwin G, Rushford K, Haysom H E and Wood E M 2020 Is platelet expiring out of date? A systematic review *Transfus. Med. Rev.* **34** 42–50
[14] Toner R W, Pizzi L, Leas B, Ballas S K, Quigley A and Goldfarb N I 2011 Costs to hospitals of acquiring and processing blood in the US: a survey of hospital-based blood banks and transfusion services *Appl. Health Econ. Health Policy* **9** 29–37
[15] The University of Mississippi, M. c. Blood product utilization guidelines
[16] Hofmann A, Ozawa S and Shander A 2021 Activity-based cost of platelet transfusions in medical and surgical inpatients at a US hospital *Vox Sang.* **116** 998–1004
[17] Prowse C V, de Korte D, Hess J R and van der Meer P F 2014 Commercially available blood storage containers *Vox Sang.* **106** 1–13
[18] Hadjesfandiari N, Schubert P, Fallah Toosi S, Chen Z, Culibrk B, Ramirez-Arcos S, Devine D V and Brooks D E 2016 Effect of texture of platelet bags on bacterial and platelet adhesion *Transfusion* **56** 2808–18
[19] Hadjesfandiari N, Weinhart M, Kizhakkedathu J N, Haag R and Brooks D E 2018 Development of antifouling and bactericidal coatings for platelet storage bags using dopamine chemistry *Adv. Healthcare Mater.* **7** 1700839
[20] Jackson S P 2007 The growing complexity of platelet aggregation *Blood* **109** 5087–95
[21] Weber M, Steinle H, Golombek S, Hann L, Schlensak C, Wendel H P and Avci-Adali M 2018 Blood-contacting biomaterials: in vitro evaluation of the hemocompatibility *Front. Bioeng. Biotechnol.* **6** 99
[22] Reviakine I, Jung F, Braune S, Brash J L, Latour R, Gorbet M and van Oeveren W 2017 Stirred, shaken, or stagnant: what goes on at the blood–biomaterial interface *Blood Rev.* **31** 11–21
[23] Gibbins J M 2004 Platelet adhesion signalling and the regulation of thrombus formation *J. Cell Sci.* **117** 3415–25

[24] Baser O, Supina D, Sengupta N and Li W 2011 Anticoagulation bridging therapy patterns in patients undergoing total hip or total knee replacement in a us health plan: real-world observations and implications *Am. Health Drug Benefits* **4** 240
[25] Jaffer I H, Fredenburgh J C, Hirsh J and Weitz J I 2015 Medical device-induced thrombosis: what causes it and how can we prevent it? *J. Thromb. Haemost.* **13** S72–S81
[26] Park J B and Lakes R S 2007 Soft tissue replacement—II: blood interfacing implants *Biomaterials* (Springer) pp 331–67
[27] Baumgartner H R, Muggli R, Tschopp T B and Turitto V T 1976 Platelet adhesion, release and aggregation in flowing blood: effects of surface properties and platelet function *Thromb. Haemost.* **35** 124–38
[28] Ratner B D 2007 The catastrophe revisited: blood compatibility in the 21st century *Biomaterials* **28** 5144–7
[29] Park S, Kim D, Park S, Kim S, Lee D, Kim W and Kim J 2018 Nanopatterned scaffolds for neural tissue engineering and regenerative medicine *Adv. Exp. Med. Biol.* **1078** 421–43
[30] Shekaran A and Garcia A J 2011 Nanoscale engineering of extracellular matrix-mimetic bioadhesive surfaces and implants for tissue engineering *Biochim. Biophys. Acta* **1810** 350–60
[31] Apte G, Hirtz M and Nguyen T-H 2022 FluidFM-based fabrication of nanopatterns: promising surfaces for platelet storage application *ACS Appl. Mater. Interfaces* **14** 24133–43
[32] Van Der Meer P F, Kerkhoffs J L, Curvers J, Scharenberg J, De Korte D, Brand A and De Wildt-Eggen J 2010 In vitro comparison of platelet storage in plasma and in four platelet additive solutions, and the effect of pathogen reduction: a proposal for an in vitro rating system *Vox Sang.* **98** 517–24
[33] Berganza E, Apte G, Vasantham S K, Nguyen T-H and Hirtz M 2022 Integration of biofunctional molecules into 3D-printed polymeric micro-/nanostructures *Polymers* **14** 1327
[34] Ventrici De Souza J, Liu Y, Wang S, Dörig P, Kuhl T L, Frommer J and Liu G Y 2018 Three-dimensional nanoprinting via direct delivery *J. Phys. Chem.* B **122** 956–62